Status of three-neutrino oscillations after the SNO-salt data

M. Maltoni,[1,*] T. Schwetz,[2,†] M. A. Tórtola,[1,‡] and J. W. F. Valle[1,§]

[1]*Instituto de Física Corpuscular-CSIC/Universitat de València, Edificio Institutos de Paterna, Apartado 22085, E-46071 Valencia, Spain*
[2]*Theoretische Physik, Physik Department, Technische Universität München, James-Franck-Strasse D-85748 Garching, Germany*

We perform a global analysis of neutrino oscillation data in the framework of three neutrinos, including the recent improved measurement of the neutral current events at the Sudbury Neutrino Observatory. In addition to all current solar neutrino data, we take into account the reactor neutrino data from KamLAND and CHOOZ, the atmospheric neutrino data from Super-Kamiokande and MACRO, as well as the first spectral data from the K2K long baseline accelerator experiment. The up-to-date best-fit values and allowed ranges of the three-flavor oscillation parameters are determined from these data. Furthermore, we discuss in detail the status of the small parameters $\alpha \equiv \Delta m^2_{\text{sol}}/\Delta m^2_{\text{atm}}$ and $\sin^2\theta_{13}$, which fix the possible strength of CP-violating effects in neutrino oscillations.

I. INTRODUCTION

Recently, the Sudbury Neutrino Observatory (SNO) experiment [1] has released an improved measurement with enhanced neutral current sensitivity due to neutron capture on salt, which has been added to the heavy water in the SNO detector. This adds precious information to the large amount of data on neutrino oscillations published in the past few years. Thanks to this growing body of data, a rather clear picture of the neutrino sector is starting to emerge. In particular, the results of the KamLAND reactor experiment [2] have played an important role in confirming that the disappearance of solar electron neutrinos [3–13], the long-standing solar neutrino problem, is mainly due to oscillations and not to other types of neutrino conversions [14,15]. Moreover, KamLAND has pinned down that the oscillation solution to the solar neutrino problem is the large mixing angle (LMA) Mikheyev-Smirnov-Wolfenstein (MSW) solution [16–19] characterized by the presence of matter effects [20,21]. On the other hand, experiments with atmospheric neutrinos [22–27] show strong evidence in favor of $\nu_\mu \to \nu_\tau$ oscillations, in agreement with the first data from the K2K accelerator experiment [28]. Together with the nonobservation of oscillations in reactor experiments at a baseline of about 1 km [29,30], and the strong rejection against transitions involving sterile states [31], this positive evidence can be very naturally accounted for within a three-neutrino framework. The large and nearly maximal mixing angles indicated by the solar and atmospheric neutrino data samples, respectively, come as a surprise for particle physics, as it contrasts with the small angles characterizing the quark sector.

In this work, we report on the implications of the new SNO-salt measurement on the determination of three-neutrino oscillation parameters. Since the SNO neutral current data accurately determine the flux of the ^{8}B neutrinos in the three-neutrino framework, we no longer assume *a priori* the standard solar model (SSM) values of Ref. [32] for the eight solar neutrino fluxes. However, these predictions and their correlated uncertainties are still taken into account in our fit, by means of an improved version of the pull-approach analysis described in Ref. [33]. In Sec. II, we investigate the impact of the new data on the solar neutrino parameters by performing a fit to solar data and the KamLAND reactor experiment in a simple two-neutrino framework. In Sec. III, we present the results of the general three-neutrino fit to the global data from solar, atmospheric, reactor, and accelerator neutrino experiments. After fixing our notation in Sec. III A, we investigate the impact of three-flavor effects on solar neutrino parameters (Sec. III B) and we give the current best-fit points and allowed ranges for all three-flavor oscillation parameters (Sec. III C). Furthermore, in Sec. III D we discuss in detail the constraints on the small parameters $\sin^2\theta_{13}$ and the ratio $\Delta m^2_{\text{sol}}/\Delta m^2_{\text{atm}}$, which are the crucial parameters governing the possible strength of CP-violating effects in neutrino oscillations. A summary of the constraints on three-neutrino oscillation parameters from all current experiments is given in Sec. IV.

II. TWO-NEUTRINO ANALYSIS OF SOLAR AND KAMLAND DATA

In this section, we investigate the impact of the new SNO-salt data on the determination of the solar neutrino parameters $\sin^2\theta_{\text{sol}}$ and Δm^2_{sol} in a two-neutrino framework. Before presenting the global analysis of all solar data, it is instructive to determine the restrictions on solar neutrino oscillation parameters that follow from SNO data only. The regions delimited by the lines in Fig. 1 are obtained only from the new SNO-salt data in the form of the neutral current (NC), charged current (CC), and elastic scattering (ES) fluxes as reported in Ref. [1]. To include these data, we follow the prescription given in Ref. [34], taking carefully into account correlations and systematic effects. The shaded regions of Fig. 1 result from the total SNO data including the new salt measurements [1], as well as the 2002 spectral day/night data

*Electronic address: maltoni@ific.uv.es
†Electronic address: schwetz@ph.tum.de
‡Electronic address: mariam@ific.uv.es
§Electronic address: valle@ific.uv.es
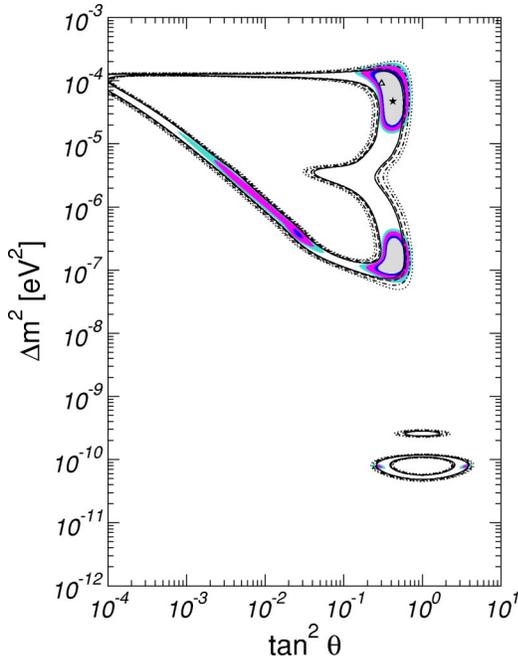
FIG. 1. Allowed regions of $\sin^2 \theta_{sol}$ and Δm^2_{sol} at 90%, 95%, 99%, and 3σ C.L. for 2 d.o.f. from SNO-salt data [1] only (lines) and total SNO data [1,11,12] (shaded regions).

[11,12]. Following Ref. [34], the 2002 and 2003 data are treated uncorrelated. For details of our SNO spectral analysis, see Ref. [31]. One sees that Fig. 1 is in good agreement with the result obtained in Ref. [1]. This figure shows also that other experiments play an important role in ruling out
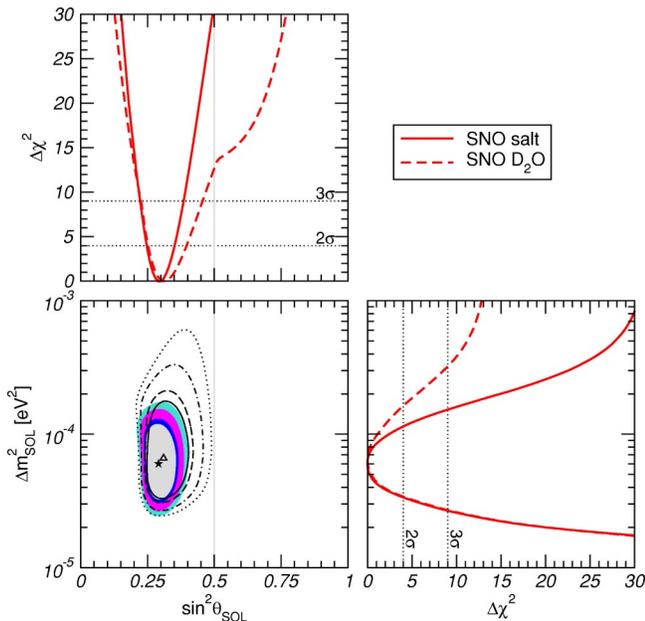
FIG. 2. Projections of the allowed regions from all solar neutrino data at 90%, 95%, 99%, and 3σ C.L. for 2 d.o.f. onto the plane of $\sin^2 \theta_{sol}$ and Δm^2_{sol} before (lines) and after (shaded regions) the inclusion of the SNO-salt data. Also shown in $\Delta \chi^2$ as a function of $\sin^2 \theta_{sol}$ and Δm^2_{sol}, minimized with respect to the undisplayed parameter.
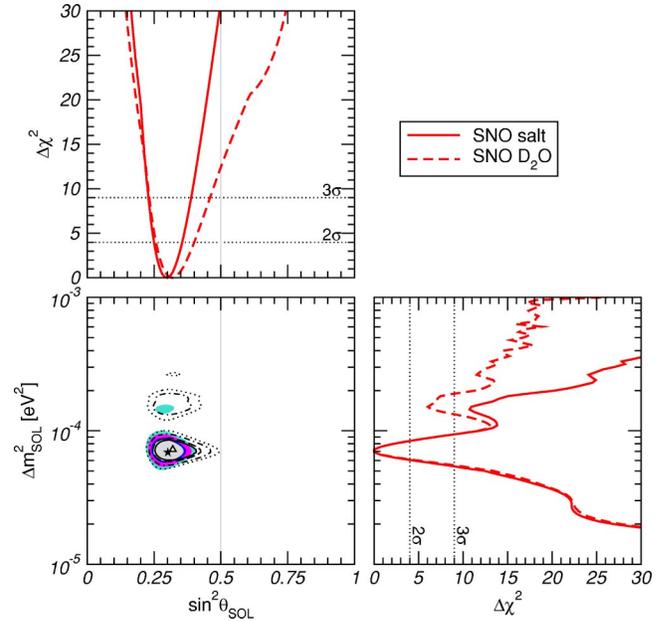
FIG. 3. Projections of the allowed regions from all solar neutrino and KamLAND data at 90%, 95%, 99%, and 3σ C.L. for 2 d.o.f. onto the plane of $\sin^2 \theta_{sol}$ and Δm^2_{sol} before (lines) and after (shaded regions) the inclusion of the SNO-salt data. Also shown is $\Delta \chi^2$ as a function of $\sin^2 \theta_{sol}$ and Δm^2_{sol}, minimized with respect to the undisplayed parameter.

low-mass solutions, such as the LOW solution, the small mixing angle nonadiabatic branch of the MSW plot, as well as the vacuum type solutions, still present here at the 99% C.L.

With this calibration at hand, we now turn to the full two-neutrino data analysis of the global set of solar neutrino data. In addition to the SNO data, we take into account the rates of the chlorine experiment at the Homestake mine [3,4] $(2.56 \pm 0.16 \pm 0.16$ SNU), the most up-to-date results [35] of the gallium experiments SAGE [5,6] $(69.1 ^{+4.3}_{-4.2} {}^{+3.8}_{-3.4}$ SNU) and GALLEX/GNO [7–9] $(69.3 \pm 4.1 \pm 3.6)$, as well as the 1496-day Super-Kamiokande data sample [10] in the form of 44 bins (eight energy bins, six of which are further divided into seven zenith angle bins). The analysis methods used here are similar to the ones described in Refs. [31], [36] and references therein, with the exception that in the current work we use the so-called pull approach for the χ^2 calculation. As described in Ref. [33], each systematic uncertainty is included by introducing a new parameter in the fit and adding a penalty function to the χ^2. However, the method described in Ref. [33] is extended in two respects. First, it is generalized to the case of correlated statistical errors [37], as is necessary to treat the SNO-salt data. Second, in the calculation of the total χ^2, we use the exact relation between the theoretical predictions and the pulls associated to the solar neutrino fluxes, rather than keeping only the terms up to first order. This is particularly relevant for the case of the solar ^{8}B flux, which is constrained by the new SNO data with an accuracy better than the prediction of the standard solar model [32]. In our approach, it is possible to take into account on the same footing both the SSM boron flux pre-
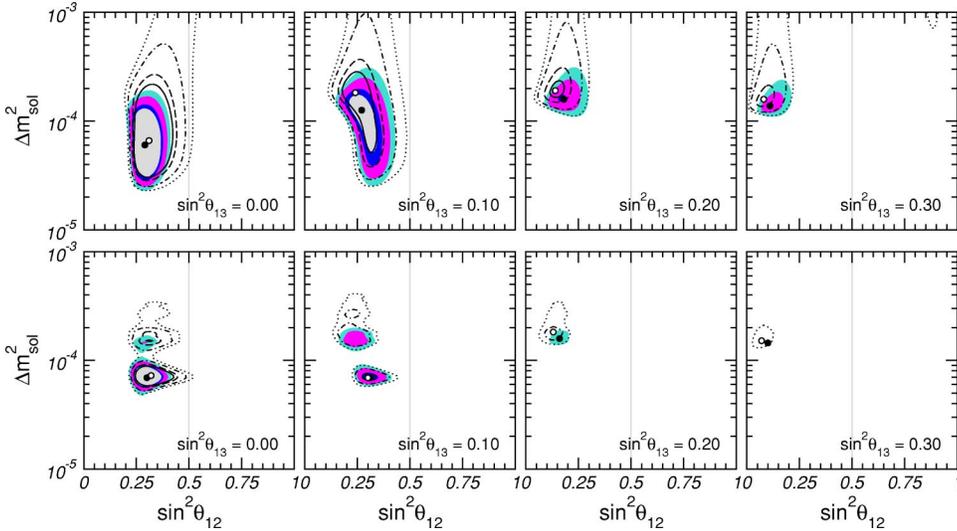
FIG. 4. Sections of the three-dimensional allowed regions in the $(\sin^2 \theta_{\text{sol}}, \Delta m^2_{\text{sol}})$ plane at 90%, 95%, 99%, and 3σ C.L. for 3 d.o.f. for various $\sin^2 \theta_{13}$ values from solar data (top) and solar +KamLAND data (bottom), before (lines) and after (shaded regions) the SNO-salt data. The local minima in each plane after (before) SNO-salt data are marked by filled (open) dots.

diction and the SNO NC measurement, without preselecting one particular value. In this way, *the fit itself* can choose the best compromise between the SNO NC data and the SSM value.

In Fig. 2, we compare the allowed regions for the oscillation parameters before and after the new SNO-salt data. One finds that especially the upper part of the LMA-MSW region and large mixing angles are strongly constrained by the new data. This follows mainly from the rather small measured value of the CC/NC ratio of $0.306 \pm 0.026 \pm 0.024$ [1], since this observable increases when moving to larger values of Δm^2_{sol} and/or $\sin^2 \theta_{\text{sol}}$ (see, e.g., Ref. [19]). The best-fit values for the parameters are

$$\sin^2 \theta_{\text{sol}} = 0.29,$$

$$\Delta m^2_{\text{sol}} = 6.0 \times 10^{-5} \ \text{eV}^2 \quad (\text{solar data}). \tag{1}$$

The new data show a much stronger rejection against maximal solar mixing: from the $\Delta \chi^2$ projected onto the $\sin^2 \theta_{\text{sol}}$ axis shown in Fig. 2 we find that $\sin^2 \theta_{\text{sol}} = 0.5$ is excluded at more than 5σ, ruling out all bimaximal models of neutrino mass [38].

We now turn to the combination of solar data with data from the KamLAND reactor experiment [2]. To this aim, we use the event-by-event likelihood analysis for the KamLAND data as described in Ref. [39], which gives stronger constraints than a χ^2-fit based on energy-binned data. In Fig. 3, we show the results of the combined analysis. Comparing post- and pre-SNO-salt results (see, e.g., Refs. [16–19]), one finds that the new data disfavor the high Δm^2 region, which appears only at the 99.5% C.L. ($\Delta \chi^2 = 10.7$).[1] The best-fit point of the global analysis occurs at

---

[1]Recently, an improved determination of the day/night asymmetry in the 1496-day Super-Kamiokande data has been released [40], which leads to a further disfavoring of the high-LMA region. Currently not enough information is available to reproduce this result outside the Super-Kamiokande Collaboration. Therefore, the day/night data are treated as in our previous analyses [31].

$$\sin^2 \theta_{\text{sol}} = 0.30, \quad \Delta m^2_{\text{sol}} = 6.9 \times 10^{-5} \ \text{eV}^2$$

$$(\text{solar} + \text{kamLAND data}). \tag{2}$$

We note that for the first time it is possible to obtain meaningful bounds on solar neutrino parameters at the 5σ level, showing that neutrino physics enters the high-precision age. From the projections of the χ^2 onto the Δm^2_{sol} and $\sin^2 \theta_{\text{sol}}$ axes also shown in Fig. 3, we find the following allowed ranges at 3σ (5σ) for 1 d.o.f.:

$$0.23 \ (0.17) \lesssim \sin^2 \theta_{\text{sol}} \lesssim 0.39 \ (0.47),$$

$$5.4 \ (2.1) \times 10^{-5} \ \text{eV}^2 \lesssim \Delta m^2_{\text{sol}} \lesssim 9.4 \ (28) \times 10^{-5} \ \text{eV}^2. \tag{3}$$

III. GLOBAL THREE-NEUTRINO ANALYSIS

A. Notations

In this section, the three-neutrino oscillation parameters are determined from a global analysis of the most recent neutrino oscillation data. For earlier three-neutrino analyses, see Refs. [18,36,41]. To fix the notation, we define the neutrino mass-squared differences $\Delta m^2_{\text{sol}} \equiv \Delta m^2_{21} \equiv m^2_2 - m^2_1$ and $\Delta m^2_{\text{atm}} \equiv \Delta m^2_{31} \equiv m^2_3 - m^2_1$, and use the standard parametrization [42,43] for the leptonic mixing matrix,

$$U = \begin{pmatrix} c_{13}c_{12} & s_{12}c_{13} & s_{13} \\ -s_{12}c_{23} - s_{23}s_{13}c_{12} & c_{23}c_{12} - s_{23}s_{13}s_{12} & s_{23}c_{13} \\ s_{23}s_{12} - s_{13}c_{23}c_{12} & -s_{23}c_{12} - s_{13}s_{12}c_{23} & c_{23}c_{13} \end{pmatrix}, \tag{4}$$

where $c_{ij} \equiv \cos \theta_{ij}$ and $s_{ij} \equiv \sin \theta_{ij}$. Furthermore, we use the notations $\theta_{12} \equiv \theta_{\text{sol}}$ and $\theta_{23} \equiv \theta_{\text{atm}}$. Because of the hierarchy $\Delta m^2_{\text{sol}} \ll \Delta m^2_{\text{atm}}$, it is a good approximation to set $\Delta m^2_{\text{sol}} = 0$ in the analysis of atmospheric and K2K data,[2] and to set Δm^2_{atm} to infinity for the analysis of solar and KamLAND data. This

---

[2]See Ref. [44] for a two-mass scale analysis of atmospheric data.
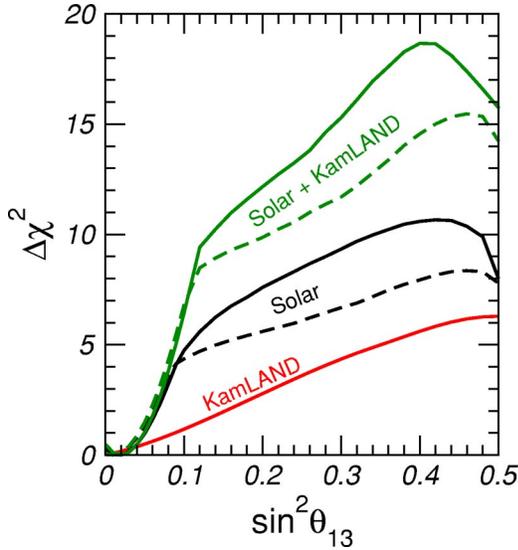
FIG. 5. $\Delta\chi^2$ profiles projected onto the $\sin^2\theta_{13}$ axis, for solar and KamLAND data, before (dashed lines) and after (solid lines) the SNO-salt experiment.

implies furthermore that the effect of a possible Dirac *CP*-violating phase [43] in the lepton mixing matrix can be neglected.[3] We perform a general fit to the global data in the five-dimensional parameter space s_{12}^2, s_{23}^2, s_{13}^2, Δm_{21}^2, Δm_{31}^2, and show projections onto various one- or two-dimensional subspaces.

B. Three-flavor solar neutrino oscillations

In this subsection, we generalize the analysis of solar and KamLAND data presented in Sec. II to three-neutrino flavors. Under the assumption of infinite Δm_{atm}^2, only the new parameter θ_{13} appears for these data (see e.g., Ref. [36]). In Fig. 4, we show the results of a three-parameter fit ($\sin^2\theta_{sol}$, Δm_{sol}^2, $\sin^2\theta_{13}$) to solar and KamLAND data. Allowed regions are shown for various values of $\sin^2\theta_{13}$ in the ($\sin^2\theta_{sol}$, Δm_{sol}^2) plane with respect to the global minimum, which occurs for $\sin^2\theta_{13} = 0.02$ including SNO-salt data, and for $\sin^2\theta_{13} = 0.01$ without the new data. Note that here we calculate the allowed regions at a given confidence level for 3 d.o.f. From this figure one finds that the new SNO-salt data contribute to the disappearance of allowed regions when $\sin^2\theta_{13}$ increases. A comparison of the allowed regions before and after the SNO-salt data shows that their size is drastically reduced for all displayed values of $\sin^2\theta_{13}$.

In Fig. 5, we show the $\Delta\chi^2$ projected onto the $\sin^2\theta_{13}$ axis for various data samples. From this figure, one can observe an improvement on the constraint on $\sin^2\theta_{13}$ thanks to the new SNO-salt data for values of $\sin^2\theta_{13} \gtrsim 0.08$. The shape of $\Delta\chi^2$ can be understood from Fig. 4: From the upper panels of that figure, one sees that increasing θ_{13} can be compensated to some extent by increasing Δm_{sol}^2. Since the

---

[3]The two Majorana phases [43] do not show up in oscillations but do appear in lepton-number-violating processes [45].

TABLE I. Best-fit values, 2σ, 3σ, and 5σ intervals (1 d.o.f.) for the three-flavor neutrino oscillation parameters from global data including solar, atmospheric, reactor (KamLAND and CHOOZ), and accelerator (K2K) experiments.

Parameter	Best fit	2σ	3σ	5σ
Δm_{21}^2 (10^{-5} eV^2)	6.9	6.0–8.4	5.4–9.5	2.1–28
Δm_{31}^2 (10^{-3} eV^2)	2.6	1.8–3.3	1.4–3.7	0.77–4.8
$\sin^2\theta_{12}$	0.30	0.25–0.36	0.23–0.39	0.17–0.48
$\sin^2\theta_{23}$	0.52	0.36–0.67	0.31–0.72	0.22–0.81
$\sin^2\theta_{13}$	0.006	$\leqslant 0.035$	$\leqslant 0.054$	$\leqslant 0.11$

new SNO-salt data disfavor large values of Δm_{sol}^2, the bound improves. Also KamLAND data act in a similar way. Since the minimum around $\Delta m_{sol}^2 \sim 7 \times 10^{-5}$ eV^2 is preferred, the "jump" of the local minimum into the high-LMA-MSW region, which is visible in the lower panels of Fig. 4 and which leads to the kink in the $\Delta\chi^2$ shown in Fig. 5, occurs at larger values of $\sin^2\theta_{13}$. We have also verified explicitly that assumptions regarding the statistical treatment of the solar boron flux have a rather small effect on these results. Finally we note that, as will be seen in Sec. III D, the bound resulting from CHOOZ and atmospheric data still dominates the overall constraint on $\sin^2\theta_{13}$ in the global analysis.

C. Global analysis of solar, atmospheric, reactor, and accelerator data

In addition to the solar and KamLAND data described so far, we now include all the charged-current atmospheric neu-
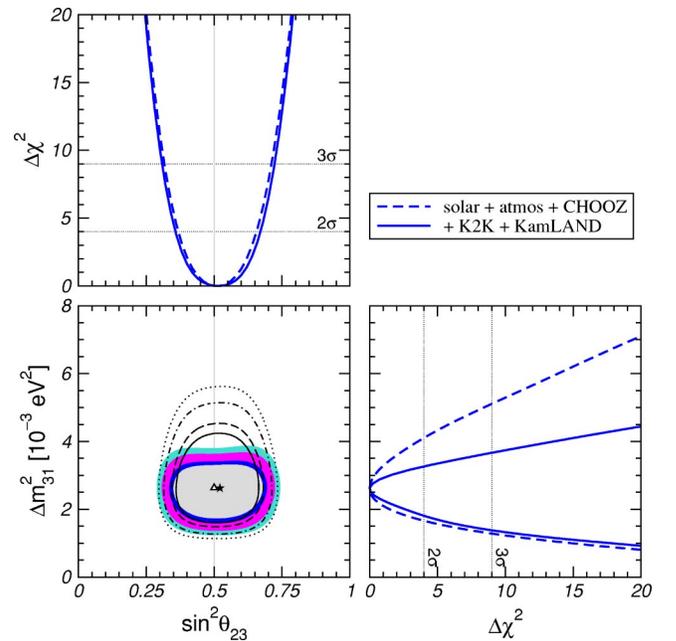
FIG. 6. Projections of the allowed regions at 90%, 95%, 99%, and 3σ C.L. for 2 d.o.f. onto the plane of $\sin^2\theta_{atm} \equiv \sin^2\theta_{23}$ and $\Delta m_{atm}^2 \equiv \Delta m_{31}^2$. The regions delimited by the lines correspond to atmospheric+solar+CHOOZ data; for the shaded regions, K2K and KamLAND data are added. Also shown is the $\Delta\chi^2$ as a function of $\sin^2\theta_{atm}$ and Δm_{atm}^2, minimized with respect to all undisplayed parameters.
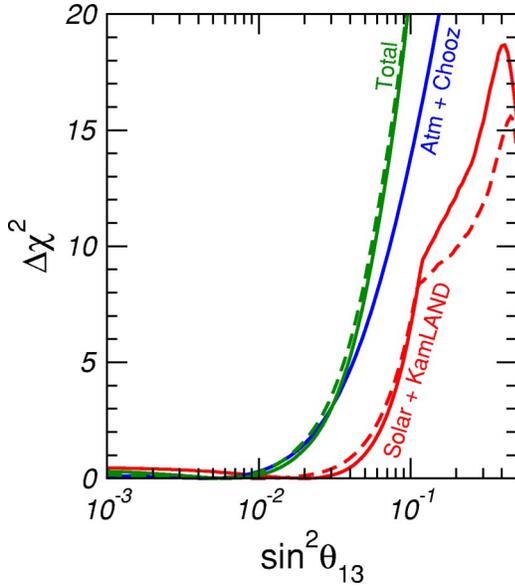
FIG. 7. $\Delta\chi^2$ profiles projected onto the $\sin^2\theta_{13}$ axis, for solar + KamLAND, atmospheric+CHOOZ, and for the global data before (dashed lines) and after (solid lines) the SNO-salt experiment.

FIG. 8. Allowed regions in the ($\sin^2\theta_{13}, \Delta m^2_{atm}$) plane at 90%, 95%, 99%, and 3σ from CHOOZ data alone (lines) and CHOOZ + solar + KamLAND data (shaded regions).

trino data, such as the most recent ones of the Super-Kamiokande [25,26] and MACRO [27] experiments. The Super-Kamiokande data include the e-like and μ-like data samples of sub- and multi-GeV contained events (10 bins in zenith angle), as well as the stopping (five angular bins) and through-going (10 angular bins) upgoing muon data events. As previously, we do not use the information on ν_τ appearance, multiring μ, and neutral-current events since an efficient Monte Carlo simulation of these data would require more detailed knowledge of the Super-Kamiokande experiment, and in particular of the way the neutral-current signal is extracted from the data. From MACRO we use the through-going muon sample divided in 10 angular bins [27]. For details of our analysis, see Refs. [31], [36] and references therein. Furthermore, we include the first spectral data from the K2K long-baseline accelerator experiment [28]. We use the 29 single-ring muon events, grouped into six energy bins, and we perform a spectral analysis similar to the one described in Ref. [46]. Finally, we take into account in our fit the constraints from the CHOOZ reactor experiment [29]. The best-fit values and the allowed intervals of the parameters s^2_{12}, s^2_{23}, s^2_{13}, Δm^2_{21}, Δm^2_{31} from the global data are given in Table I. This table summarizes the current status of the three-flavor neutrino oscillation parameters.

For completeness, we show in Fig. 6 the projection of the allowed regions from the global fit onto the plane of the atmospheric neutrino parameters. We find that the first 29 events from K2K included here start already to constrain the upper region of Δm^2_{atm}. We note that recently the Super-Kamiokande Collaboration has presented a preliminary re-analysis of their atmospheric data [47]. The update includes changes in the detector simulation, data analysis, and input atmospheric neutrino fluxes. These changes lead to a slight downward shift of the mass splitting to the best-fit value of $\Delta m^2_{atm} = 2\times10^{-3}$ eV.[2] Currently it is not possible to re-

cover enough information from Ref. [47] to incorporate the corresponding changes in our codes. We note, however, that the quoted value for Δm^2_{atm} is statistically compatible with our result. For $\Delta m^2_{atm} = 2\times10^{-3}$ eV^2 and maximal mixing, we obtain a $\Delta\chi^2 = 1.3$.
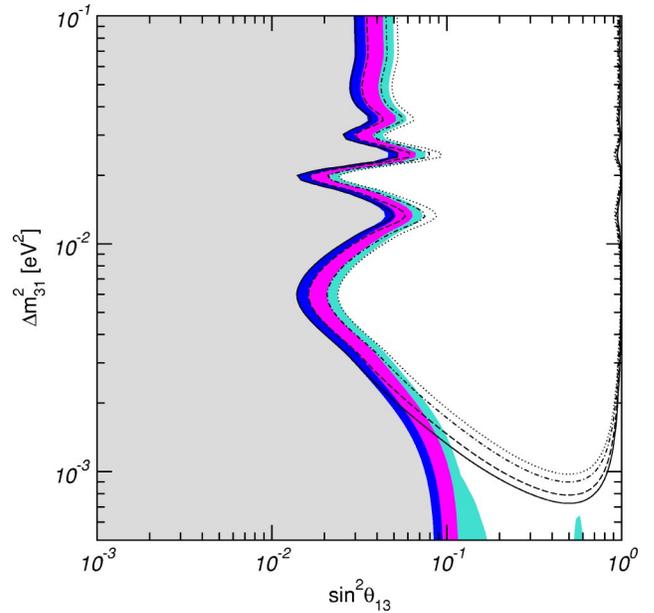
D. Status of θ_{13} and the mass hierarchy parameter $\alpha = \Delta m^2_{sol}/\Delta m^2_{atm}$

In this subsection, we discuss in detail the current information on the small parameters relevant for subleading oscillation effects. First we consider the mixing angle θ_{13}, which at the moment is the last unknown angle in the three-neutrino mixing matrix. Only an upper bound exists, which used to be dominated by the CHOOZ reactor experiment [29]. Currently a large effort is being made to determine this angle in future experiments (see, e.g., Refs. [38,48,49]).

In Fig. 7, we show the $\Delta\chi^2$ as a function of $\sin^2\theta_{13}$ for different data sample choices. One can see how the bound on $\sin^2\theta_{13}$ as implied by the CHOOZ experiment in combination with the atmospheric neutrino data still provides the main restriction on $\sin^2\theta_{13}$. We find the following bounds at 90% C.L. (3σ) for 1 d.o.f.:

$$\sin^2\theta_{13} \lesssim \begin{cases} 0.070 \ \ (0.12) & (\text{solar}+\text{KamLAND}) \\ 0.028 \ \ (0.066) & (\text{CHOOZ}+\text{atmospheric}) \\ 0.029 \ \ (0.054) & (\text{global data}) \end{cases}$$

(5)

However, we note that the solar data contribute in an important way to the constraint on $\sin^2\theta_{13}$ for lower values of Δm^2_{atm}. In particular, the downward shift of Δm^2_{atm} reported in Ref. [47] implies a significant loosening of the CHOOZ bound on $\sin^2\theta_{13}$, since this bound gets quickly weak when
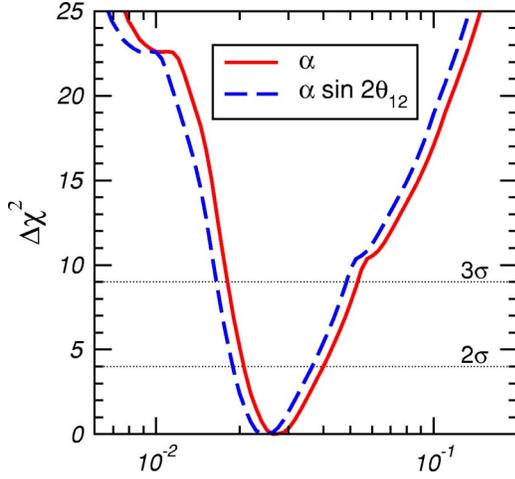
FIG. 9. $\Delta\chi^2$ from global oscillation data as a function of $\alpha \equiv \Delta m^2_{sol}/\Delta m^2_{atm}$ and $\alpha \sin 2\theta_{12}$.

Δm^2_{atm} decreases (see, e.g., Ref. [50]). Such loosening in sensitivity is prevented to some extent by solar neutrino data. In Fig. 8, we show the allowed regions in the $(\sin^2\theta_{13}, \Delta m^2_{atm})$ plane from an analysis including solar and reactor neutrino data (CHOOZ and KamLAND). One finds that, although for larger Δm^2_{atm} values the bound on $\sin^2\theta_{13}$ is dominated by the CHOOZ+atmospheric data, for low $\Delta m^2_{atm} \simeq 10^{-3}$ eV^2 the solar+KamLAND bound is comparable to that coming from CHOOZ+atmospheric.

For example, fixing $\Delta m^2_{atm} = 2 \times 10^{-3}$ eV^2, we obtain at 90% C.L. (3σ) for 1 d.o.f. the bound

$$\sin^2\theta_{13} \lesssim 0.035 \quad (0.066) \quad (\Delta m^2_{atm} = 2 \times 10^{-3} \text{ eV}^2), \quad (6)$$

which is slightly worse than the bound from global data shown in Eq. (5).

For the exploration of genuine three-flavor effects such as *CP* violation, the mass hierarchy parameter $\alpha \equiv \Delta m^2_{sol}/\Delta m^2_{atm}$ is of crucial importance since, in a three-neutrino scheme, *CP* violation disappears in the limit where two neutrinos become degenerate [51]. Therefore, we show in Fig. 9 the $\Delta\chi^2$ from the global data as a function of this parameter. Also shown in this figure is the $\Delta\chi^2$ as a function of the parameter combination $\alpha \sin 2\theta_{12}$, since to leading order in the long baseline $\nu_e \rightarrow \nu_\mu$ oscillation probability, solar parameters appear in this particular combination [52]. We obtain the following best-fit values and 3σ intervals:

$$\alpha = 0.026, \quad 0.018 \leq \alpha \leq 0.053,$$

$$\alpha \sin 2\theta_{12} = 0.024, \quad 0.016 \leq \alpha \sin 2\theta_{12} \leq 0.049.$$
$$(7)$$

IV. CONCLUSIONS

We have performed a global analysis of neutrino oscillation data in the three-neutrino scheme, including the recent improved measurement of the neutral current events at SNO. We include in our fit all current solar neutrino data, reactor neutrino data from KamLAND and CHOOZ, the atmospheric neutrino data from Super-Kamiokande and MACRO, as well as the first data from the K2K long-baseline accelerator experiment. We have discussed the implications of the improved neutral current measurement on the determination of the solar neutrino oscillation parameters. The SNO-salt results reject the previously allowed high-mass branch of Δm^2_{sol} at about 3σ. Moreover, it rules out maximal solar mixing at more than 5σ, precluding the possibility of bimaximal models of neutrino mixing.

Furthermore, we have determined the current best-fit values and allowed ranges for the three-flavor oscillation parameters from the global oscillation data. Our three-neutrino re-
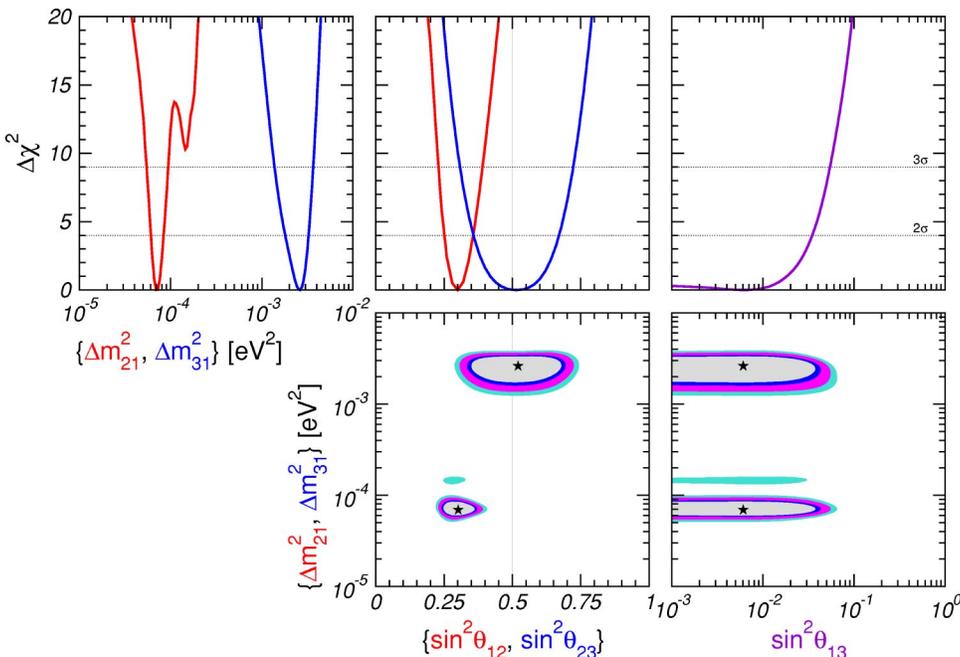
FIG. 10. Projections of the allowed regions from the global oscillation data at 90%, 95%, 99%, and 3σ C.L. for 2 d.o.f. for various parameter combinations. Also shown is $\Delta\chi^2$ as a function of the oscillation parameters $\sin^2\theta_{12}$, $\sin^2\theta_{23}$, $\sin^2\theta_{13}$, Δm^2_{21}, Δm^2_{31}, minimized with respect to all undisplayed parameters.

sults are summarized in Table I and in Fig. 10, showing the allowed regions and χ^2 projections for the five oscillation parameters $\sin^2 \theta_{sol}$, $\sin^2 \theta_{atm}$, $\sin^2 \theta_{13}$, Δm^2_{sol}, Δm^2_{atm}. In addition, we have discussed in detail the limits on the small mixing angle $\sin^2 \theta_{13}$, as well as the hierarchy parameter $\alpha = \Delta m^2_{sol} / \Delta m^2_{atm}$. These small parameters are relevant for genuine three-flavor effects, and restrict the magnitude of leptonic *CP* violation that one may potentially probe at future experiments such as superbeams or neutrino factories. In particular, we have seen how the improvement on the $\sin^2 \theta_{13}$ limit that follows from the new SNO-salt data solar neutrino experiments cannot yet match the sensitivity on $\sin^2 \theta_{13}$ reached at reactor experiments. However, the solar data do play an important role in stabilizing the constraint on $\sin^2 \theta_{13}$ with respect to variation of Δm^2_{atm}. For small enough Δm^2_{atm}

values, the solar data probe $\sin^2 \theta_{13}$ at a level comparable to that of the current reactor experiments.

ACKNOWLEDGMENTS

[1] SNO Collaboration, S. N. Ahmed *et al.*, ''Measurement of the Total Active 8B Solar Neutrino Flux at the Sudbury Neutrino Observatory with Enhanced Neutral Current Sensitivity,'' nucl-ex/0309004.

[2] KamLAND Collaboration, K. Eguchi *et al.*, Phys. Rev. Lett. **90**, 021802 (2003).

[3] B. T. Cleveland *et al.*, Astrophys. J. **496**, 505 (1998).

[4] R. Davis, Prog. Part. Nucl. Phys. **32**, 13 (1994).

[5] SAGE Collaboration, J. N. Abdurashitov *et al.*, J. Exp. Theor. Phys. **95**, 181 (2002).

[6] SAGE Collaboration, J. N. Abdurashitov *et al.*, Phys. Rev. C **60**, 055801 (1999).

[7] GALLEX Collaboration, W. Hampel *et al.*, Phys. Lett. B **447**, 127 (1999).

[8] GNO Collaboration, M. Altmann *et al.*, Phys. Lett. B **490**, 16 (2000).

[9] GNO Collaboration, C. M. Cattadori, Nucl. Phys. B (Proc. Suppl.) **110**, 311 (2002).

[10] Super-Kamiokande Collaboration, S. Fukuda *et al.*, Phys. Lett. B **539**, 179 (2002).

[11] SNO Collaboration, Q. R. Ahmad *et al.*, Phys. Rev. Lett. **89**, 011301 (2002).

[12] SNO Collaboration, Q. R. Ahmad *et al.*, Phys. Rev. Lett. **89**, 011302 (2002).

[13] SNO Collaboration, Q. R. Ahmad *et al.*, Phys. Rev. Lett. **87**, 071301 (2001).

[14] M. Guzzo *et al.*, Nucl. Phys. **B629**, 479 (2002).

[15] J. Barranco, O. G. Miranda, T. I. Rashba, V. B. Semikoz, and J. W. F. Valle, Phys. Rev. D **66**, 093009 (2002).

[16] M. Maltoni, T. Schwetz, and J. W. F. Valle, Phys. Rev. D **67**, 093003 (2003).

[17] J. N. Bahcall, M. C. Gonzalez-Garcia, and C. Pena-Garay, J. High Energy Phys. **02**, 009 (2003).

[18] G. L. Fogli *et al.*, Phys. Rev. D **67**, 073002 (2003).

[19] P. C. de Holanda and A. Y. Smirnov, J. Cosmol. Astropart. Phys. **02**, 001 (2003).

[20] L. Wolfenstein, Phys. Rev. D **17**, 2369 (1978).

[21] S. P. Mikheev and A. Y. Smirnov, Sov. J. Nucl. Phys. **42**, 913 (1985).

[22] Kamiokande Collaboration, Y. Fukuda *et al.*, Phys. Lett. B **335**, 237 (1994).

[23] IMB Collaboration, R. Becker-Szendy *et al.*, Nucl. Phys. B (Proc. Suppl.) **38**, 331 (1995).

[24] Soudan-2 Collaboration, W. W. M. Allison *et al.*, Phys. Lett. B **449**, 137 (1999).

[25] M. Shiozawa, Talk at Neutrino 2002, http://neutrino2002.ph.tum.de/.

[26] Super-Kamiokande Collaboration, Y. Fukuda *et al.*, Phys. Rev. Lett. **81**, 1562 (1998).

[27] MACRO Collaboration, A. Surdo, Nucl. Phys. B (Proc. Suppl.) **110**, 342 (2002).

[28] K2K Collaboration, M. H. Ahn *et al.*, Phys. Rev. Lett. **90**, 041801 (2003).

[29] CHOOZ Collaboration, M. Apollonio *et al.*, Phys. Lett. B **466**, 415 (1999).

[30] F. Boehm *et al.*, Phys. Rev. D **64**, 112001 (2001).

[31] M. Maltoni, T. Schwetz, M. A. Tortola, and J. W. F. Valle, Phys. Rev. D **67**, 013011 (2003) (hep-ph/0207227 v3 KamLAND-updated version).

[32] J. N. Bahcall, S. Basu, and M. H. Pinsonneault, Phys. Lett. B **433**, 1 (1998); J. N. Bahcall, M. H. Pinsonneault, and S. Basu, Astrophys. J. **555**, 990 (2001).

[33] G. L. Fogli, E. Lisi, A. Marrone, D. Montanino, and A. Palazzo, Phys. Rev. D **66**, 053010 (2002).

[34] SNO HOWTO kit, Q. R. Ahmad *et al.*, http://www.sno.phy.queensu.ca/sno/.

[35] H. Robertson, Talk at the TAUP03 conference, 2003, Seattle, Washington, http://mocha.phys.washington.edu/taup2003/.

[36] M. Gonzalez-Garcia, M. Maltoni, C. Pena-Garay, and J. W. F. Valle, Phys. Rev. D **63**, 033005 (2001).

[37] A. B. Balantekin and H. Yuksel, Phys. Rev. D (to be published), hep-ph/0309079.

[38] For recent reviews, see S. Pakvasa and J. W. F. Valle, hep-ph/0301061, prepared for Special Issue of Proceedings of the Indian National Academy of Sciences on Neutrinos; V. Barger, D. Marfatia, and K. Whisnant, hep-ph/0308123, and references therein.

[39] T. Schwetz, hep-ph/0308003.

[40] Super-Kamiokande Collaboration, M. B. Smy *et al.*, hep-ex/0309011.

[41] M. C. Gonzalez-Garcia and C. Pena-Garay, Phys. Rev. D (to be published), hep-ph/0306001.

[42] Particle Data Group, K. Hagiwara *et al.*, Phys. Rev. D **66**, 010001 (2002).

[43] J. Schechter and J. W. F. Valle, Phys. Rev. D **22**, 2227 (1980).

[44] M. C. Gonzalez-Garcia and M. Maltoni, Eur. Phys. J. C **26**, 417 (2003).

[45] M. Doi, T. Kotani, H. Nishiura, K. Okuda, and E. Takasugi, Phys. Lett. **102B**, 323 (1981). J. Schechter and J. W. Valle, Phys. Rev. D **23**, 1666 (1981); **24**, 1883 (1981); **25**, 283(E) (1982).

[46] G. L. Fogli, E. Lisi, A. Marrone, and D. Montanino, Phys. Rev. D **67**, 093006 (2003).

[47] Super-Kamiokande Collaboration, Y. Hayato, Talk at the HEP2003 conference (Aachen, Germany, 2003), http:// eps2003.physik.rwth-aachen.de

[48] P. Huber, M. Lindner, T. Schwetz, and W. Winter, Nucl. Phys. **B665**, 487 (2003).

[49] P. Huber, M. Lindner, and W. Winter, Nucl. Phys. **B645**, 3 (2002); M. Apollonio *et al.*, hep-ph/0210192; Muon Collider/ Neutrino Factory Collaboration, M. M. Alsharoa *et al.*, Phys. Rev. ST Accel. Beams **6**, 081001 (2003).

[50] G. L. Fogli, E. Lisi, A. Marrone, D. Montanino, A. Palazzo, and A. M. Rotunno, Phys. Rev. D (to be published), hep-ph/0308055.

[51] J. Schechter and J. W. Valle, Phys. Rev. D **21**, 309 (1980).

[52] M. Freund, Phys. Rev. D **64**, 053003 (2001).